CO ADSORPTION ON VARIOUS OXIDE PHASES GROWN ON PALLADIUM(111) AND ISOTHERMAL OXIDATION ON PdO(101)

By

TAO LI

A THESIS PRESENTED TO THE GRADUATE SCHOOL
OF THE UNIVERSITY OF FLORIDA IN PARTIAL FULFILLMENT
OF THE REQUIREMENTS FOR THE DEGREE OF
MASTER OF SCIENCE

UNIVERSITY OF FLORIDA

2014

To Quanning, Feng, and my family

ACKNOWLEDGMENTS

I sincerely thank to my advisor, Dr. Jason Weaver for his guidance and encouragement. I gratefully acknowledge my committee member, Dr. Helena Hagelin-Weaver for her interest in my education. I particularly thank Feng Zhang for his helpful discussion and experimental support. I also want to acknowledge John T. Diulus, Rahul Rai, Dr. Can Hakanoglu for their valuable advices.

On a personal point, I thank my family for their financial and mental support throughout these years. I also thank my boyfriend for his strong encouragement and letting me know what is truly important in my life. I thank all my friends I met during these two years master study, you guys are unbelievable.

TABLE OF CONTENTS

LIST OF FIGURES

Abstract of Thesis Presented to the Graduate School
of the University of Florida in Partial Fulfillment of the
Requirements for the Degree of Master of Science

CO ADSORPTION ON VARIOUS OXIDE PHASES GROWN ON PALLADIUM(111) AND ISOTHERMAL OXIDATION ON PdO(101)

By

Tao Li

May 2014

Chair: Jason F. Weaver
Major: Chemical Engineering

CO molecule, due to its simple vibrational and electronic structure, makes itself an ideal candidate for the investigation of vibrational spectroscopy on transition metals and their oxide surfaces. In this thesis, I will present two studies that were conducted during my two years master research at University of Florida.

The first study focuses on the investigation of oxidation on Pd(111) surface. Temperature programmed desorption (TPD) of two-dimensional (2D) oxide and PdO(101) were obtained under the Ultra high vacuum (UHV) condition and oxygen uptake curve was collected at the temperature before and after precursor desorption peak. Because the initial formation of PdO(101) surface is mediated by the stability of precursor state, and at high temperature the uptake curve abruptly slows down at ~0.7ML. Thus we used this phenomenon to calibrate the oxygen coverage scale in this experiment.

The second study focuses on the Reflection-Absorption Infrared Spectroscopy (RAIRS) spectra of CO adsorption on Pd(111) and oxidized surface as well as isothermal oxidation of CO on PdO(101) surface. It turns out that at 100 K CO adsorbs on bridge and hollow sites on Pd(111) at the saturation coverage of 0.5 ML, whereas for Pd_5O_4 and PdO(101) surface, CO mainly adsorbs on mixture of atop and bridge sites at saturation coverage of 0.46 ML and 0.35 ML,

respectively. Isothermal CO oxidation experiment shows the change of CO characteristic adsorption peak as the decrease of oxygen surface coverage.

CHAPTER 1
INTRODUCTION

Background and Motivation

Palladium oxide is one of the important heterogeneous oxidation catalysts for commercial oxidation processes, such as catalytic combustion of methane in lean gas turbines, oxidation of CO in automotive exhausts and so forth. Improving the performance of those processes as well as the necessity of energy conservation motivate us to fully investigate the fundamental understanding of the mechanism of palladium and its oxide growth, as well as the chemical property of oxide phase on metal surface. CO oxidation is one of the simplest and most widely studied catalytic reactions in heterogeneous catalysis, its highly facile reactivity towards palladium and palladium oxide makes it an ideal model for the study of elementary surface processes.

Various techniques and methods can be employed in the characterization of palladium and its oxide as well as the study of CO oxidation. In this study, TPD, RAIRS and density functional theory (DFT) calculations are used. Other techniques such as low energy electron diffraction (LEED), scanning tunneling microscopy (STM) will be employed in the future work.

By using atomic oxygen beam, we have been now successfully extend the range of oxygen concentrations on palladium surface under UHV condition, which enable us to conduct detail investigation on bulk oxide phase, therefor obtain new information about the fundamental details of the properties of oxidized surface and the its essentially role in the oxidation catalysis.

Plasma Source Characterization

As one of the important facilities, plasma source is used for routinely sample cleaning and making oxide. Thus, the characterization of plasma source will give us a clear idea about the range of operational condition for utilization. We fed pure O_2 to generate plasma and

characterized the resulting beams using line-of-sight mass spectrometry to determine the beam composition as a function of oxygen pressure. We also investigated the oxidation of Pd(111) at specific plasma conditions (200W, 9 millitorr O_2) to estimate the O-atom flux at the sample.

Figure 1-1 shows the O-atom fraction in the beam as a function of O_2 partial pressure in the plasma for 150 W to 240 W radio frequency (RF) power input. The O-atom fraction represents the fraction of the total species (O and O_2) in the beam that are O-atoms. As we can see from Figure 1-1, the O-atom fraction decreases with O_2 partial pressure in the plasma chamber and increase with RF power, but latter will influence more comparing with former. Note that we limit the RF power to 240 W to be conservative and partial pressure to 10 millitorr at 150 W in case that plasma would extinguish.

Figure 1-2 shows the O-atom flux estimated at sample surface. The sample was held at an angle of about 45°, 29.2 cm away from the plasma source. As we can see, the atomic flux increases monotonically with O_2 partial pressure above 200 W whereas appears to pass through a maximum at 200 W and lower RF power. At our normal operation condition (9 millitorr and 200 W), the estimated O-atom flux is 0.0043 ML/s, where $1ML=1.5\times10^{15}$ atoms/cm^2.

Experimental Techniques

UHV environment is the starting point for utilization of all other facilities. Several pumping techniques are used for achieving the base pressure of 2×10^{-10} torr, mainly due to the different operation range of different types of pumps as well as large pressure change that occurs in the chambers. There are four types of pumps utilized in the lab, along with an additional "bake out" procedure to obtain low base pressure.

The first level of obtaining UHV condition is by setting roughing pumps to achieving 1×10^{-3} torr such that it is suitable for the implementation of other high vacuum pumps. Roughing

pump operates by applying compression mechanism to displace gas from the vacuum system. The second level is achieved by using turbomolecular pump, which is connected to the roughing pump for reaching base pressure of 1×10^{-7} torr -1×10^{-8} torr. Turbomolecular pump rotates a set of blades at a high speed and the gas molecules are hit from the inlet towards the outlet of the pump to create higher vacuum. Another two pumps, ion pumps and titanium sublimation pump (TSP), help to achieve the third level of UHV. Former one ionizes gas molecules in a vessel which is applied by strong electrical potential, and this high potential accelerates the ionized molecules to be captured by the wall of the pump. This type of pump is capable of reaching base pressure of 10^{-11} torr. TSP consists of three titanium filaments and by sublimating them, a thin coat film will be coated surrounding the chamber wall. Since clean titanium is very reactive, it will react with gas molecules colliding on the wall and form a stable product, thus maintaining the low pressure.

TPD

TPD is a surface technique that quantitatively provides the information about kinetics of desorption molecules from the surface when surface temperature is increased. Whereas another similar technique, temperature program reaction spectroscopy (TPRS), monitors desorption species with additional reactions occurring on the surface as increasing surface temperature. These two techniques are carried out by first dosing the species of interest on the surface, followed by heating the surface in a constant rate (1 K/s) while monitoring the desorbents that either directly desorbs from the surface or desorbs after reactions. A quadropole mass spectrometer (QMS) is used for detecting and monitoring in this case. Typically, the signal of desorbents is plotted as a function of surface temperature in TPD spectrum, thus the activation energies can be deduced because desorption temperature reveals the amount of energy that is required for breaking surface bond.

Due to the large pumping speed and low heating rate, desorption rate can be assumed to proportional to the desorption pressure [1]. Redhead provided a method for providing the kinetics of surface processes in his 1963 paper [2-3], in which he showed that desorption rate could be expressed by the following equation:

$$\frac{r_d}{N_s} = -\frac{d\theta_A}{dt} = k_o \theta_A^n \exp(-\frac{E_A}{KT}) \quad (1\text{-}1)$$

Where r_d is desorption rate of species A, N_s is surface sites concentration, θ_A is the coverage of species A, t is time, k_o is pre-exponential of rate constant, n is desorption order, E_A is activation energy of desorption reaction, K is Boltzmann's constant, T is surface temperature. After taking the first derivative of equation (1-1) and rearranging, the maximum desorption rate can be found in the following equation:

$$\frac{E_A}{KT_P} = ln\left(\frac{k_o T_p n \theta_p^{n-1}}{\beta_H}\right) - ln\left(\frac{E_A}{kT_p}\right) \quad (1\text{-}2)$$

Where T_p is maximum desorption peak temperature, β_H is heating rate, θ_p is the coverage at peak maxima. From equation 1-2, if n=1, then the peak temperature would be independent with surface coverage, whereas if n=2, the initial coverage would influence the desorption process, thus result in a shift of the temperature of desorption peak.

TPD spectra can provide us quantitative information about surface coverage. By integrating the entire curve with respect to surface temperature, and comparing with known saturation coverage that has been calibrated for the surface, one can obtain surface coverage of the adsorbent.

RAIRS

RAIRS is a surface technique that perform vibration spectrum of absorbed molecules on metal surface. Besides, due to the high sensitivity and resolution of this technique, it is especially

suitable for the study of interaction between adsorbents and metal surface as well as intermolecular interaction within the adsorbed layers.

Hoffmann [4] has already summarized IRAIS studies in a macroscopic perspective, and three considerations are important:

1. Incident light must have p-polarized component (i.e. the component parallel to the plane of incidence), and this component only vibrates with a dipole moment that is perpendicular to the metal surface.
2. A grazing incidence is necessary regarding incident light.
3. For adsorption on transition metals, usage of single reflection is preferred, thus studies should be carried out on oriented single crystals.

As illustrated by Hoffmann [4], excitation of vibrational transition by infrared light follows the rule that only vibrational transitions associated to the change in dipole moment are IR active. The intensity of IR peak can be expressed in following equation:

$$I_k \sim \left(\frac{\partial \mu}{\partial Q_k}\right) \tag{1-3}$$

Where μ is molecule dipole moment, Q_k is the normal coordinate associated to the k^{th} vibrational mode.

For adsorbed molecule, the number of IR active vibration is determined by both nonzero dipole moment change and number of internal (3N-6) modes plus hindered translational and rotational modes due to the adsorption on metal surface, where N is the number of molecule.

Crystal Structure of PdO(101) Surface

As presented in Figure 1-3, bulk PdO crystal has tetragonal unit cell which consists of square planar units of Pd atoms coordinating with four-fold oxygen atoms. The bulk-terminated PdO(101) surface investigated in this study is defined by rectangular unit cell with dimensions of a=3.043 Å and b=6.142 Å and consists of closed-packed rows of three-fold Pd (Pd_{3f}) and four-fold Pd (Pd_{4f}) arranged alternately coordinating with three-fold or four-fold oxygen atoms,

respectively. A and b lattice vectors of rectangular unit cell are labeled in the [010] and [$\bar{1}$01] directions in Figure 1-3B. Thus, half of the Pd atoms on the surface are coordinately unsaturated Pd_{cus}, which likely to be more reactive than Pd_{4f} regarding binding with adsorbed molecules. The density of palladium and oxygen surface atom is 0.7 ML, so 0.35 ML corresponds to the coverage of Pd_{cus} and O_{cus}.

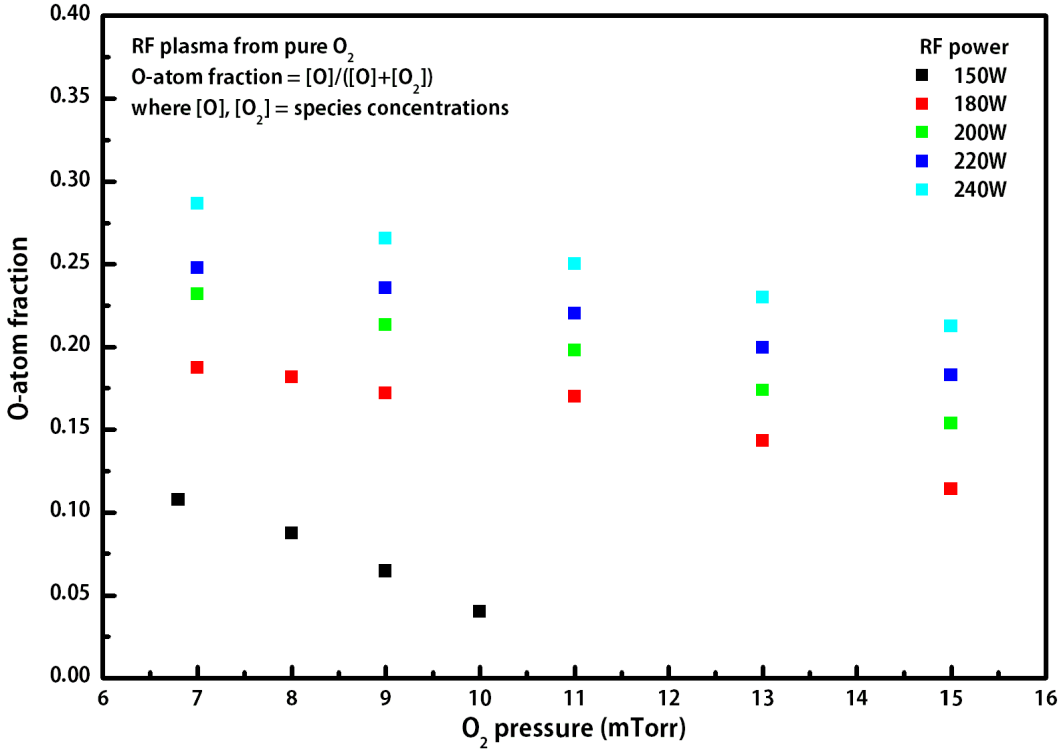

Figure 1-1. O-atom fraction in the beam as a function of O_2 partial pressure for different RF input power.

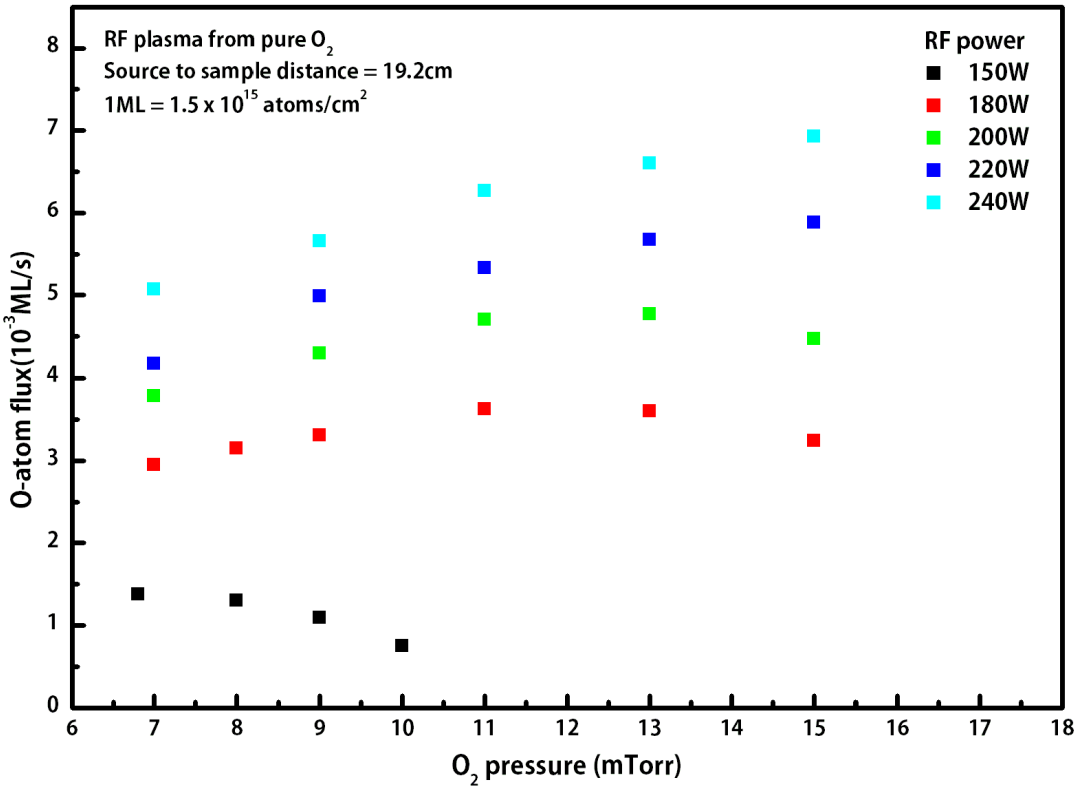

Figure 1-2. O-atom flux estimate sample surface as a function of O_2 partial pressure for different RF input power.

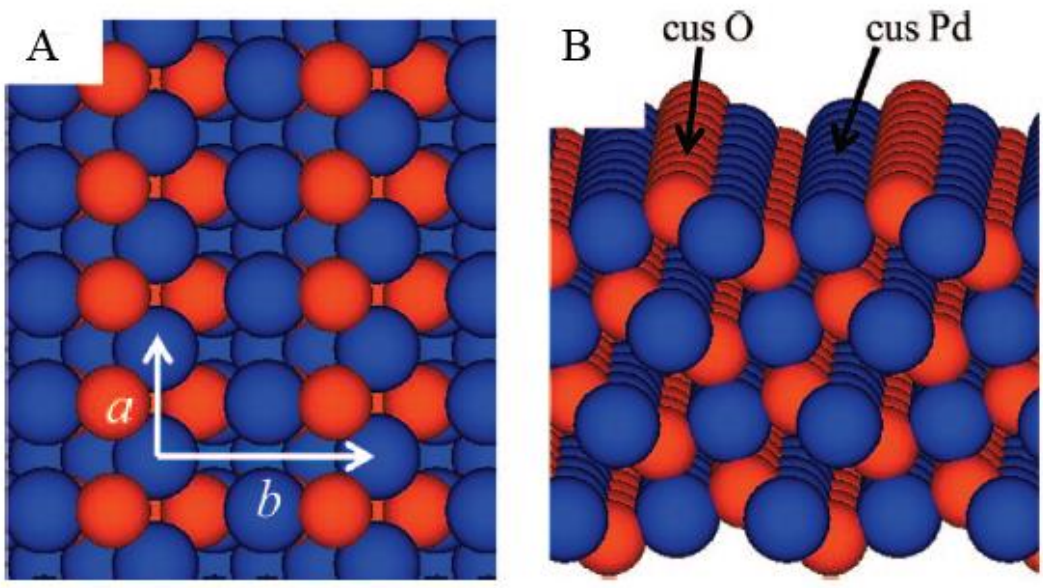

Figure 1-3. Crystal structure of PdO(101) thin film. A) Top view and B) Side view. The red and blue atoms represent O and Pd atoms, respectively. Directions a and b labeled in A) correspond to the [010] and [$\bar{1}$01] direction of PdO. 3-fold coordinated O_{cus} and Pd_{cus} rows are indicated in B).

CHAPTER 2
THE OXIDATION OF PALLADIUM (111) IN ULTRAHIGH VACUUM

Palladium (111) Oxidation Motivation

The oxidation of Pd(111) surface to 2D oxide and PdO(101) bulk oxide plays a significant role in the determination of property of palladium catalysts in oxygen-rich applications, which include the exhaust gas such as alkane and CO remediation in automobiles [5-8], power generation plants and fuel cell catalysis. The development of oxidation of Pd(111) has been characterized well [9-17], with mainly working on the 2D surface oxide [18-26]. It was shown that a p(2×2) structure is first arranged by chemisorbed oxygen atoms at the total oxygen coverage of 0.25ML. Further surface reconstruction and formation of various 2D oxide are found at higher coverage. Lundgren and Han [27-28] reported that 2D oxide has a preferred Pd_5O_4 stoichiometry with $(\sqrt{6} \times \sqrt{6})$ structure, aligning with the [-1 1 0] directions of Pd(111) substrate, whereas other oxygen phase appear to be meta-stable relative to Pd_5O_4 surface. Furthermore, previous studies [29-32] have investigate distinct feature and property about precursor in TPD spectra of Pd(111) oxide. Briefly, a broad peak between 500K and 650K in the desorption feature arises from precursor state and initially appear at ~0.7 ML, which is the saturation coverage of 2D oxide. Atomic oxygen uptake curve has also been done by Kan [29] in different incident fluxes and surface temperature, which reveals a strongly dependency of kinetics for Pd(111) oxidation on the thermal stability of precursor state. In this study, we investigated the TPD spectra of 2D oxide and PdO(101) surface, obtained atomic oxygen uptake curves under different temperature as well as quantified oxygen surface coverage.

Experimental Methods

The experiments were conducted in an UHV system that reaches the base pressure less than 2.5×10^{-10} Torr. The chamber is evacuated by a turbomolecular pump, an ion pump and a

titanium sublimation pump that is inserted into the liquid-nitrogen cooled cryoshield. A shielded QMS, a single-stage differentially pumped beam chamber that houses a RF power plasma source for generating atomic oxygen beam and three leak valves which are used for gas-dosing are assembled in the middle of the main chamber. One side of the chamber houses a LEED/ Auger electron spectroscopy (AES). A Bruker Tensor 27 FTIR is set outside the UHV chamber and sends the mid-infrared (MIR) beam that is transmitted within a sealed box to the differentially pumped potassium bromide (KBr) window. Inside the sealed box which is continuously purged with H_2O and CO_2 free compressed air, a set of flat mirrors direct the MIR beam to a parabolic mirror that is used to focus the MIR beam onto the sample. Inside the UHV chamber, focused MIR beam impinges on the sample surface at an angle of 80° relative to the normal direction. The reflected MIR beam exits the chamber through a second KBr window and is detected by liquid N_2-cooled HgCdTe (MCT) detector using another set of focusing mirrors, all of which are in a second sealed box that is continuously purged with H_2O and CO_2 free compressed air.

The Pd(111) crystal that was used in this study is a circular disk attached to a type K thermocouple wire for temperature measurement and a high voltage wire at the backside of the crystal for electron bombardment heating. Crystal is attached to two a copper sample holder in thermal contact with a liquid nitrogen (LN) cooled reservoir. A tungsten wire is set under the back of sample without touching for radiative heating, which is controlled by a proportional-integral-derivative (PID) controller that varies the output of a programmable direct current (DC) power supply to maintain or linearly ramp the sample temperature from 91 K to 1250 K. Sample was initially cleaned by sputtering with Ar^+ ions at 700 K, followed by annealing to 1100 K. After several cycles argon sputtering, sample was exposed to an atomic oxygen beam at 823K for routinely cleaning, followed by flashing the sample to 900K. Previous study [30] has already

discussed that the limitation of sample temperature at 900K will maintain oxygen-saturation in the subsurface and will remove carbon impurities. This minimizes the possibility of losing chemisorbed oxygen because of the bulk dissolution during following TPD experiments [13], so that the reproducibility of oxygen coverage obtained by TPD will be ensured. The surface was considered to be clean when we obtained sharp LEED patterns consistent with Pd(111) surface.

In this system, gaseous oxygen atoms were produced by partially dissociating pure oxygen (Airgas 99.999%) supplied to the quartz tube at end of the plasma. We used RF power of 200 W and 9 mtorr oxygen pressure in this study. The source-to-target distance was about 29.2 cm and the sample was held at an angle of about 45° with respect to the tube axis for the measurements. We characterized the Pd(111) surface after oxidation by atomic oxygen beam at various exposure time and surface temperatures, then immediately adjusted the sample position such that the sample would face the entrance of a QMS ionizer at the distance of 2 mm, followed by increasing the temperature at a linear rate of 1 K/s.

Result and Discussion

Calibration of Oxygen Coverage

We quantify the 2D oxide and PdO(101) oxygen surface coverage by comparing integrated TPD signal areas to the area obtained after averaging several surface oxide saturation coverage that were done at similar exposure time at 583 K. Previous research [29] has already shown that at high temperature, the uptake curve abruptly slows down at ~0.7 ML surface oxide saturation coverage, which implies that the PdO formation is initially limited by the competitive desorption from precursor state. The rate of oxidation then gradually increases with atomic oxygen exposure, followed by decreasing to the PdO layer saturation coverage. An autocatalytic mechanism [29] for PdO growth can explain the acceleratory kinetics after ~0.7 ML. More specifically, as the PdO precursors grow in size, they become more stable such that less of them

undergo decomposition process and more PdO particles grow bigger, which revealed by the accelerating rate before PdO layer saturation. In this study, we obtained the O_2 TPD spectra by exposing the Pd(111) surface held at 583 K to the atomic oxygen beam under various exposure time and integrated O_2 TPD signal areas. The areas between 190 s-240 s are relatively close and we assume that this is the surface oxide saturation coverage 0.7 ML. The coverage scale is 1.1244×10^{-7} ML/C, which is calculated by using 0.7 ML divided by the average area of 190 s-240 s. Figure 2-1 shows the TPD spectra after unit transformation of y-axis from counts per second to monolayer per second. Figure 2-2 shows the oxygen coverage as a function of atomic oxygen exposure at 583 K. We only did the oxygen coverage up to 0.775 ML, because the uptake curve has already given us the TPD areas relative to ~0.7 ML to calculate the coverage scale. The estimation of oxygen atom beam flux was done by assuming the unit probability of gas-phase oxygen atoms adsorption up to 0.7 ML and fitting the early part of oxygen uptake curve with linear function. Previous studies [33] have shown that this procedure gives a reasonable estimation of beam flux.

TPD of Various Oxide Phases

Figure 2-3 shows a series of short time exposure O_2 TPD spectra collected by exposing the Pd(111) surface to gas-phase atomic oxygen at a surface temperature of 433 K. As mentioned above, the oxygen atoms will first chemisorb into a p (2×2) structure below 0.25 ML, which is revealed by the broad peak produced through recombinative desorption between 550 K and 775 K. As the oxygen coverage increase above 0.25 ML, we observe a sharp peak that shifts from 638 K to 644 K, which originates from the autocatalytic decomposition process of ordered 2D oxide [11-12]. A leading edge appears at 670 K of sharp 2D oxide peak at 0.5 ML and gradually develops into a separate peak as the increasing of desorption rate. The broad peak between 433 K

and 583 K is the feature of precursor state and previous studies [29] has already demonstrated that first appearance of this state is at ~0.7 ML saturation coverage of 2D oxide, which agrees well with this experiment. The peak near 620 K is attributed to the decomposition of bulk-like PdO domains and autocatalytic decomposition of coexisting surface oxide results in the peak near 662 K [34]. Figure 2-4 shows a series of long time exposure O_2 TPD spectra collected by exposing the Pd(111) surface to gas-phase atomic oxygen at a surface temperature of 433 K. From (a) we can see that the precursor state peak gradually diminishes as the bulk-like PdO domain continues to grow. The peak at 665 K both intensifies and shifts towards higher temperature as the PdO grows. Further increasing of the oxygen coverage leads to the intensification of bulk-like PdO domain and the peak at ~693 K without shifting toward higher temperature.

Atomic Oxygen Uptake Curve

Figure 2-2 and 2-5 reveal that thermal stability of precursor has a strong influence on the kinetics of Pd(111) oxidation. The temperatures carried out in two uptake curves lie below and above the precursor desorption peak in TPD spectra (Figure 2-3B, Figure 2-4A). Comparing with temperature at 583 K, the oxygen uptake increases monotonically with exposure at 433K until the saturation coverage at ~4.0 ML. As illustrated above, the beam flux is calculated by fitting the early part of oxygen uptake curve with linear function and the beam flux is 0.00429 ML s^{-1}. The uptake curve at 583 K, however, abruptly slows down at ~0.7 ML, which is the saturation coverage of 2D oxide, and then gradually increases with the atomic oxygen exposure. These phenomena can be explained that initially PdO formation is limited by the competitive desorption from precursor, as this state becomes more stable, the self-accelerating kinetics occurs, which leads to the increase of oxidation rate.

Summary

We calculated the oxygen calibration coverage and investigated the TPD of 2D and PdO(101) as well as oxygen uptake curve under low and high temperature using atomic oxygen beam under UHV condition. The O_2 TPD spectra characterized the evolution of 2D oxide and PdO(101) and show the development of precursor state under different oxygen coverage. The oxygen uptake curves collected at the temperature before and after precursor desorption peak give us the evidence that initial formation of PdO on the surface is mediated by the stability of precursor state, more specifically, at low temperature, the oxygen coverage increases monotonically with exposure, whereas at high temperature, the oxygen coverage initially is a linear function of exposure, but abruptly slows down at ~0.7 ML, which is the saturation coverage of 2D oxide, and then gradually increases with exposure until PdO layer saturation coverage.

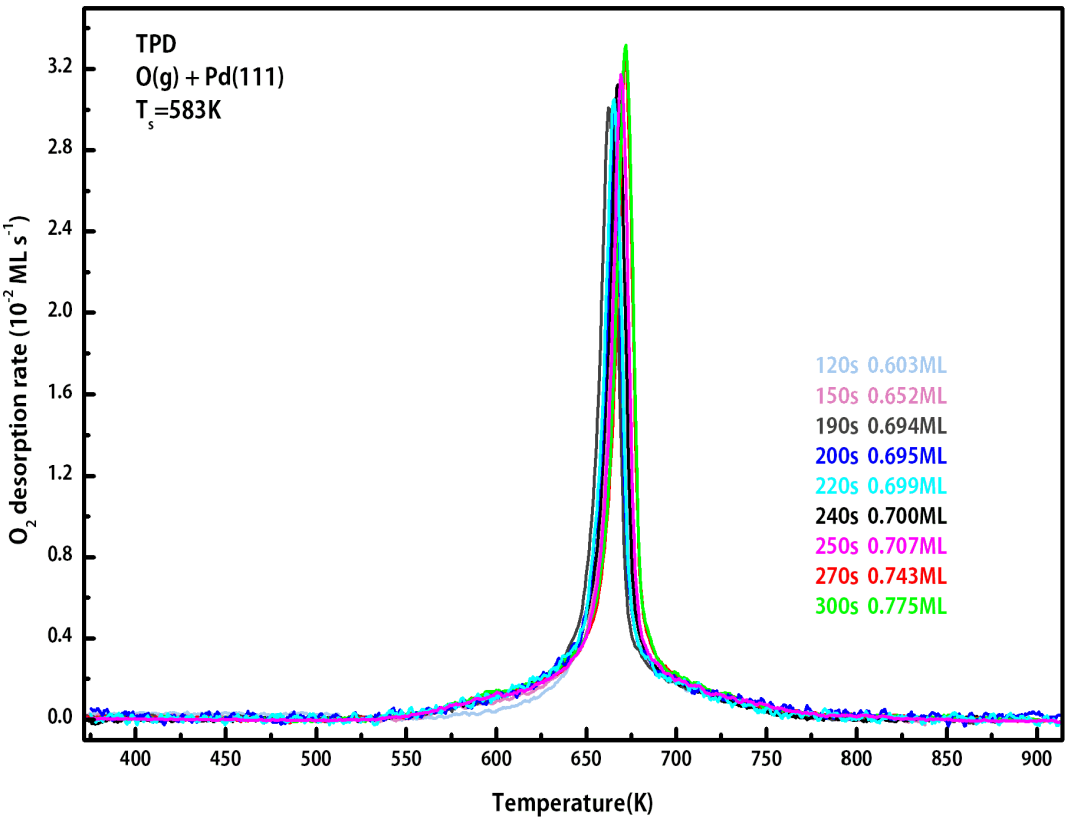

Figure 2-1. O_2 TPD spectra was obtained by exposing Pd(111) surface to atomic oxygen under various exposure time at surface temperature of 583K. The heating rate is 1K s^{-1} for all of the TPD measurements. The panel illustrates the exposure time and the relative oxygen coverage.

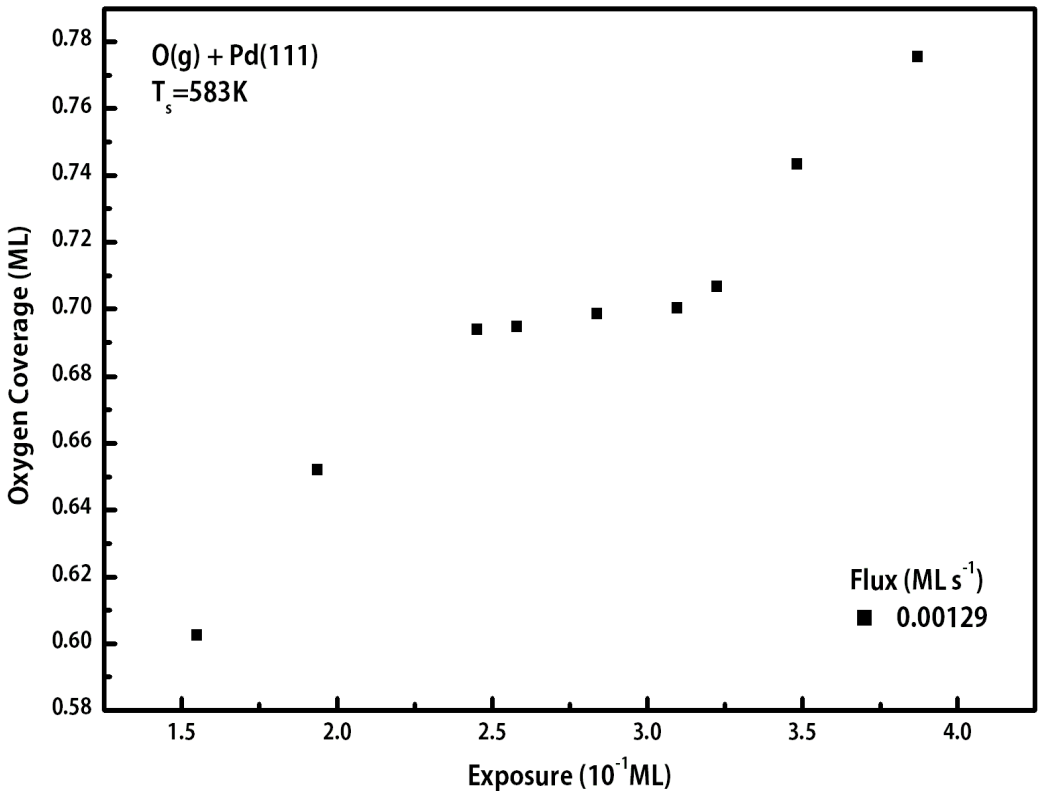

Figure 2-2. Uptake curve plotted as oxygen coverage vs. atomic oxygen exposure at the surface temperature of 583K. The unit of x-axis is ML. Beam flux illustrated in the panel is 0.00129ML s^{-1}.

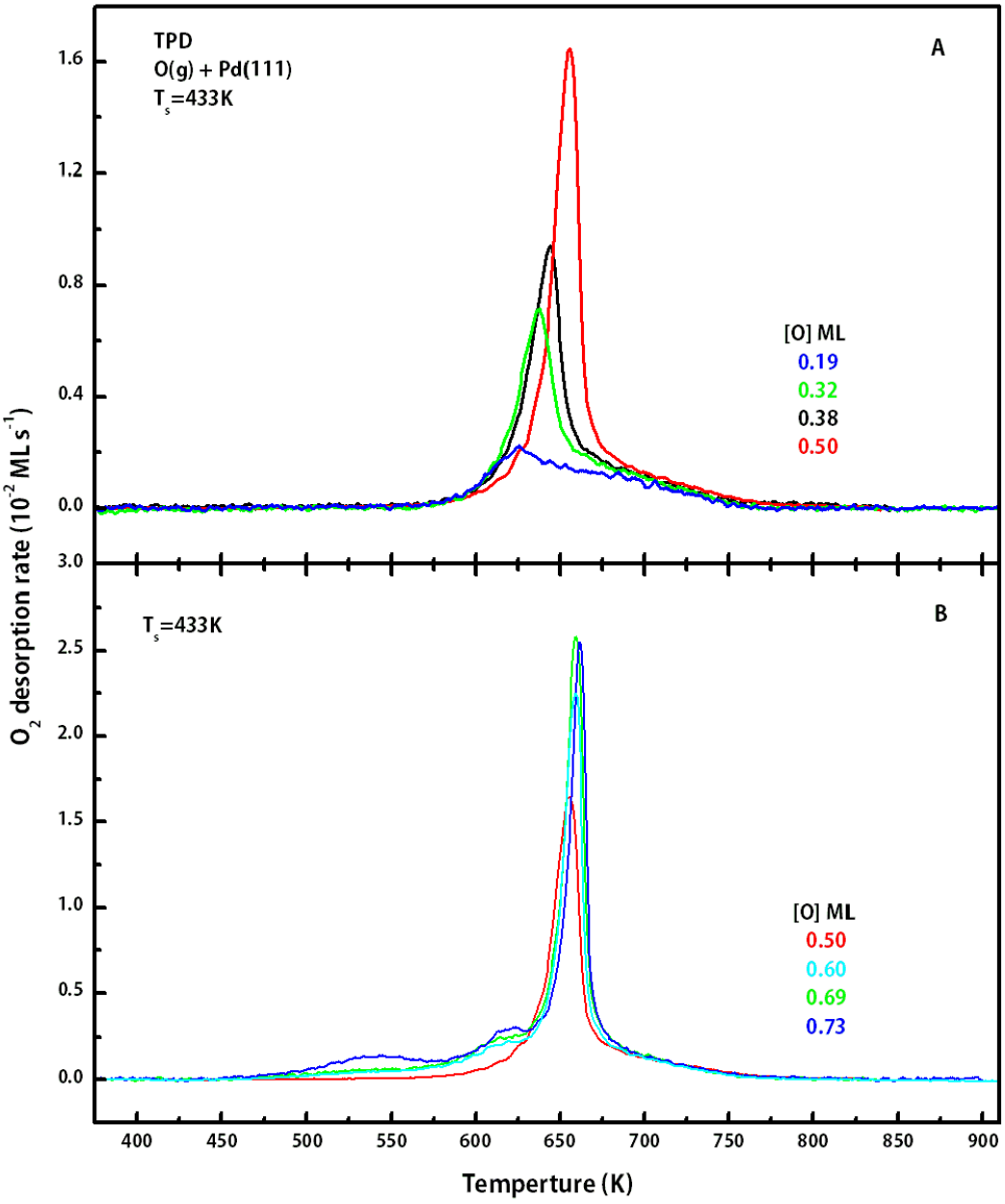

Figure 2-3. O_2 TPD short time exposure spectra was obtained by exposing Pd(111) surface to atomic oxygen under 433K. The heating rate is 1K s^{-1}. A) Oxygen coverage from chemisorbed oxygen to 2D oxide. B) 2D oxide coverage to its saturation coverage.

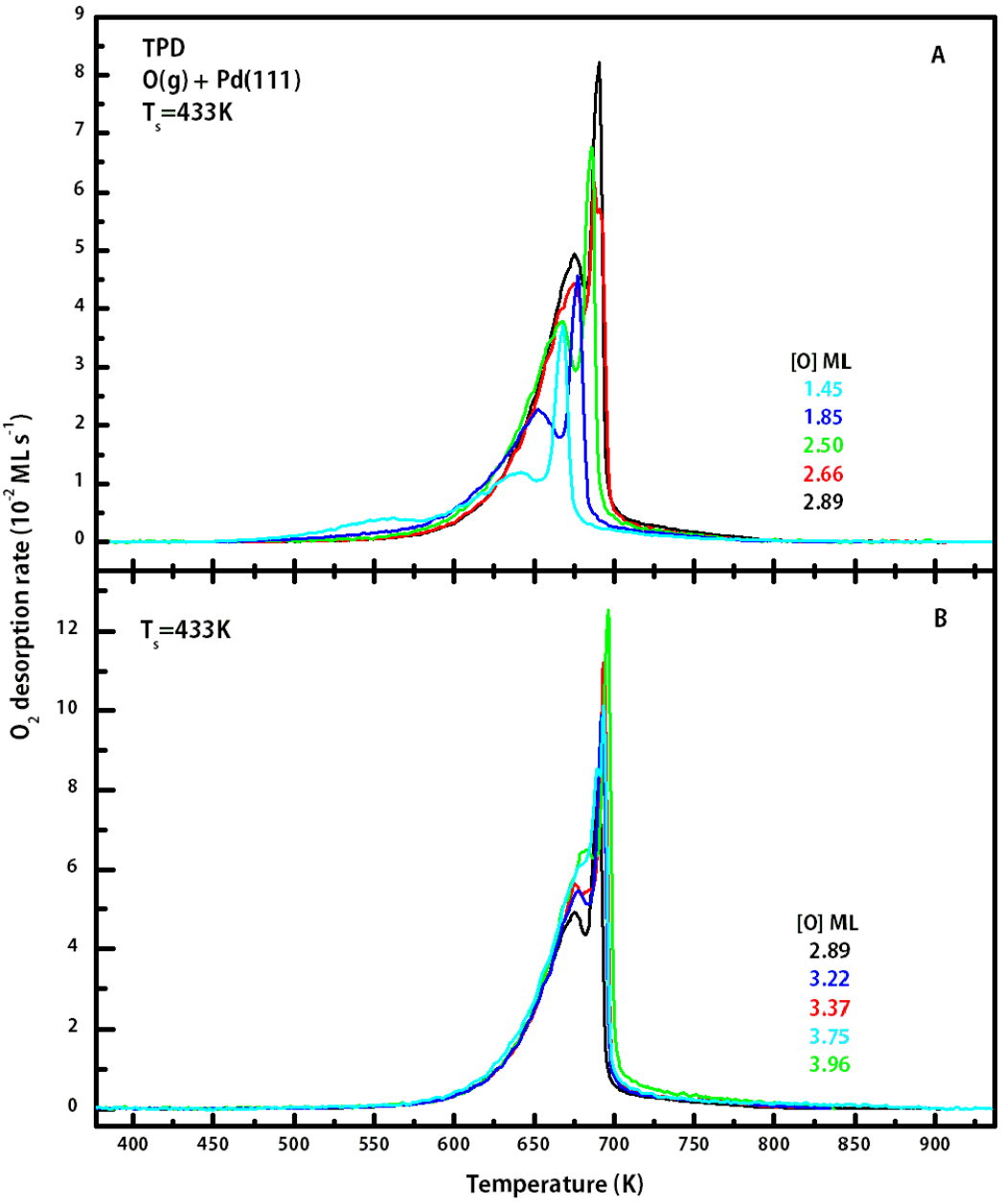

Figure 2-4. O_2 TPD long time exposure spectra was obtained by exposing Pd(111) surface to atomic oxygen under 433K. The heating rate is 1K s^{-1}.

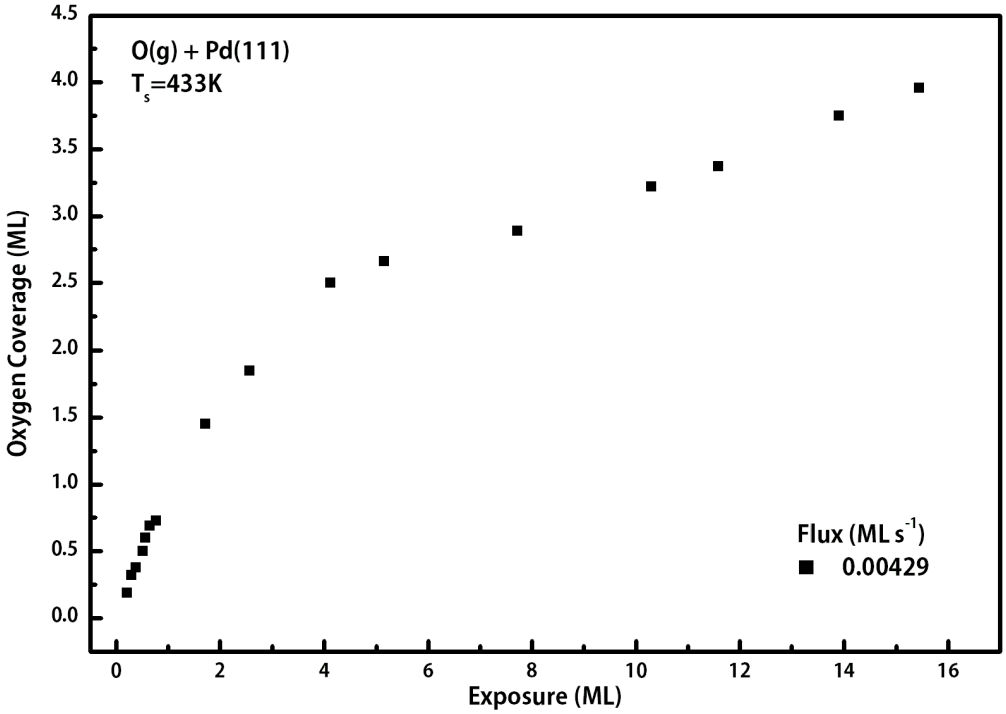

Figure 2-5. Uptake curve plotted as oxygen coverage vs. atomic oxygen exposure at the surface temperature of 433K. The unit of x-axis is ML. Beam flux illustrated in the panel is 0.00429ML s^{-1}.

CHAPTER 3
ISOTHERMAL CO OXIDATION ON PdO (101) AT 373K

CO Surface Interaction Motivation

CO oxidation is one of the most extensively investigated reactions in heterogeneous catalysis and surface science. Understanding the mechanism of this catalytic reaction is essential for reducing the amount of pollutants release by automobile exhaust and increasing the fuel economy of automobiles. Numerous studies have already been done on substrate-supported [35-36] and singe-crystal metal surface [37-39] as well as metal oxide [40], in which some of the general conclusion have been drawn. For oxidation reaction particularly, CO follows concerted mechanism [41-42] and molecularly adsorbs to the late transition metals surface via carbon atom. The oxidation proceeds between chemisorbed CO and O atoms via Langmuir-Hinshelwood mechanism and CO adsorption is the rate-determining step.

Surface reactivity can be probed through chemical reduction, during which oxide surface configuration can be changed. A variety of previous studies [43-45] have been done concerning CO adsorption on Pd single crystal and RAIRS has proved itself to be a powerful technique for providing vibrational frequency of different C-O bonding sites on the surface. Bradshaw and Hoffmann [45] assigned 2120-2050 cm^{-1} as the frequency range for CO adsorbing on the top of Pd (atop). 1950-1880 cm^{-1} is the frequency range of bridge CO interacting with two Pd atoms. 1880-1800 cm^{-1} is referred to the hollow site frequency of which CO interacts with three Pd atoms. It has been well characterized that surface structure of CO overlayers on Pd(111) are coverage dependent [43, 45-46], where CO forms $\sqrt{3} \times \sqrt{3}R30^{\circ}$ and c(4×2) -2CO at 0.33 ML and 0.5 ML respectively, saturates at 0.75 ML by forming (2×2) – 3CO compressed structure. Previous studies [4, 43, 45] have indicated that at 0.33 ML, CO adsorbs in 3-fold hollow sites whereas at 0.75 ML, CO occupies both 3-fold hollow and atop sites. However, the conclusion

about surface structure at 0.5ML was questioned in the later studies [47-48]. Regarding on this argument, recent study [49] shows that at 0.55 ML, CO adsorbs on both bridge and 3-fold hollow sites on Pd(111) at 100 K.

Comparing with the investigation in metal, less work has been done on palladium oxide due to the difficulty of generating well-ordered palladium oxide surfaces under UHV condition. As introduced above, the apparatus we have allow us to expose the Pd(111) crystal to highly reactive atomic oxygen and prepare the well-ordered PdO(101) surface ~3.3 ML under the main chamber pressure of $\sim 5\times10^{-9}$ torr for 30 minutes exposure. In this study, we investigated the isothermal oxidation of CO on PdO(101) surface under 373 K by using TPD and RAIRS, from which the reaction coverage and vibration frequencies were obtained. The comparison of them reveals the change in bonding site during the reaction as well as provides us more information about the kinetics of isothermal CO oxidation on PdO(101) surface.

Experimental Methods

Details about the UHV chamber and preparation of clean Pd(111) surface have already been discussed above. In the RAIRS experiment of CO adsorption on Pd(111) and oxidized Pd(111) surface, Pd(111) was cleaned by exposing to the plasma-generated atomic oxygen beam at 823 K, followed by flashing to 900 K to remove carbon contamination. Pd_5O_4 was prepared by exposing the cleaned Pd(111) surface to the atomic oxygen for 220 s at 583 K, followed by annealing to 600 K. As discussed in the chapter, this condition made the surface coverage in the so-called metastable regime and oxygen coverage is 0.7 ML. PdO(101) layers was prepared by exposing the cleaned Pd(111) surface to atomic oxygen for 30 min at 433 K and oxygen coverage is ~3.3 ML. RAIRS data were collected at 100 K after exposing the three types of surfaces to a saturate dose of CO (~10 L).

In isothermal CO oxidation experiment, the PdO(101) layer was prepared by exposing the Pd(111) crystal to the atomic oxygen for 30min at 433 K, followed by annealing to 533 K to make the surface more well-ordered, then dropped down to 100 K. During decreasing the surface temperature, the sample was positioned at a distance about 3 mm from aperture of mass spectrometer. CO was charged through a leak valve once the temperature dropped down to 100 K at main chamber pressure of 5×10^{-9} torr, and CO_2 signal was monitored to establish a baseline for 4 minutes. Then the temperature was increased at a constant rate of 1 K/s to 373 K and held for 3 minutes, followed by decreasing to 100 K. We repeated this cycle for 7 times until most of the oxide was reacted by CO. The residual oxygen coverage was collected by another TPRS experiment which was taken immediately after isothermal experiment. Sample temperature was increased at the rate of 1 K/s to 900 K at the CO background of 5×10^{-9} torr, O_2 and CO_2 signal were monitored.

In isothermal RAIRS experiment, PdO(101) layer was prepared as discussed above and sample was positioned so that mid-IR beam can be reflected through the sample surface to the detector. After the surface temperature was dropped down to 100 K, CO was charged through a leak valve once the temperature dropped down to 100 K at main chamber pressure of 5×10^{-9} torr, and CO_2 signal was monitored by the mass spectroscopy at the same time. After for running for 5 minutes at 100 K at 5×10^{-9} torr, scan the IR spectrum, followed by heating the sample to 373 K and holding for 3 minutes, then dropping back to 100 K and did another IR scan. Repeat the cycle for another 6 times, and every IR scan was obtained during 100 K sample temperature. After the 7 IR spectrum scan, sample was flashed to 900 K for 3 minutes and then dropped to 100 K to obtain the IR spectrum of CO on Pd(111) metal surface by charging CO to main chamber pressure for 5×10^{-9} torr.

Result and Discussion

RAIRS of CO Adsorption on Pd(111), Pd_5O_4 and PdO(101) Surface

RAIRS experiments of CO adsorption on metal and oxidized surface were performed to determine the site assignment at CO saturation coverage. The results are shown in Figure 3-1. For CO on Pd(111) surface, a strong peak is observed at 1960 cm^{-1} and three small peaks are apparent at 2118, 2109 and 1899 cm^{-1}. TPD measurement under this case gave us 0.53 ML CO saturation coverage and the 1960 cm^{-1} feature in our spectra has been assigned previously [4, 43-44] to the CO adsorbed on bridging sites within c(4×2) phase at 0.5 ML CO coverage. Notices that CO saturation coverage can reach 0.75 ML by forming c(2×2)-3CO phase at 100 K reported by previous studies [43-44], and the spectrum is dominated by atop peak at 2111 cm^{-1} and 1896 cm^{-1} hollow peak for CO binding within the (2×2)-3CO phase. In our case, 0.75 ML can only be achieved after annealing Pd(111) surface to 150 K while exposing to CO background and took IR scan when sample temperature dropped back to 100 K. This phenomenon was also observed by Kuhn et al [43] before. The small peaks at 2118, 2109 and 1899 cm^{-1} in this spectra indicate there are small c(2×2)-3CO compressed phase regimes within the c(4×2) phase. The DFT calculations reported recently [49] shows that the frequencies of c(4×2)-bridge+hollow structure close to our experimental results 1960 cm^{-1} and 1867 cm^{-1}.

For Pd_5O_4 surface, prior work shows that annealing the temperature to 600 K after the preparation of oxide transforms so-called metastable 2D oxide to the root 6 on Pd(111) surface. Figure 3-4 shows that the saturation coverage of CO on Pd_5O_4 is 0.46 ML at 100 K. As shown in Figure 3-1, at CO saturation coverage, IR spectra give us a strong peak at 2131 cm^{-1} and a shoulder peak at 2111 cm^{-1}, some broad peaks at 2010, 1984 and 1956 cm^{-1}, and two small peaks at 1867 and 1826 cm^{-1}. DFT frequency calculations [49] of CO adsorption on Pd_5O_4 at low and high coverage show that the dominant 2131 cm^{-1} is consistent to the atop CO, whereas 2010,

1956 and 1867 cm^{-1} is close to the frequencies of bridge CO. 1826 cm^{-1} low intensity peak can be assigned to the hollow site according to the DFT calculation. The shoulder peak appeared at 2111 cm^{-1} has been observed as atop CO on Pd(111) metal surface at compressed c(2×2)-3CO phase [43, 46] at saturation coverage 0.75 ML, which may indicate that Pd_5O_4 is imperfect and some Pd(111) regimes may exist on the surface.

For PdO(101) surface, previous TPRS study [50] has shown that CO saturation coverage is 0.35 ML, which is consistent with the concentration of coordinately unsaturated Pd (Pd_{3f}) atoms on PdO(101) surface. This coincidence indicates that CO preferentially adsorbs on the Pd_{3f} sites, and all these sites are occupied under the saturation coverage. In Figure 3-1, a dominant 2127 cm^{-1} and a broad 1954 cm^{-1} peak are observed, which correspond to atop and bridging CO respectively according to the previous [49] and recent DFT calculation (Figure 3-2). Atop-to-bridge peaks ratio is 1.65 in this case. Specifically, recent DFT calculation has been used to explore possible configurations on pristine PdO(101) surface and the preferred ones are CO adsorbing on the top of Pd_{3f} (all-atop) and atop-bridge-atop CO (t-b-t) at high coverage. According to DFT calculation, the intensity of atop vs. bridge peak is 1.09 vs. 5.73 for t-b-t configuration with which atop CO frequency is at 2143 cm^{-1} and bridge frequency is at 1953 cm^{-1}. For all-atop case, the intensity of atop CO peak is 1.05 with frequency at 2149 cm^{-1}. Based on these data, we assume that t-b-t phase and all-atop phase co-exist at saturation coverage and 90% of the species are atop CO. 36% of the surface coverage is t-b-t phase, the rest is all-atop surface. This assumption gives us 0.32 ML CO saturation coverage, which is reasonably close to previous TPRS result (0.35 ML). Notice that the frequency for atop CO in these two cases is ~2143 cm^{-1}, which is larger than 2132 cm^{-1} in spectra. The red shift of the frequency may be either caused by

the mixture of atop and bridge CO, which results in a stronger adsorption for atop CO, or the uncertainty of experimental data or DFT calculation.

Isothermal CO Oxidation on PdO(101) at 373 K

The isothermal CO oxidation spectra (Figure 3-4) were collected at the same condition under 5×10^{-9} torr CO background. In Figure 3-4A, the surface was heated to 373 K and reaction took place for 3 minutes, followed by cooling down to 100 K, wherein IR was collected (Figure 3-5). The reaction was repeated for 7 cycles until almost all the oxygen coverage was consumed (96.47%). Figure 3-4B was collected immediately after isothermal experiment, where sample was heated to 900 K at rate of 1 K/s with 5×10^{-9} torr CO background. The residual oxygen and reacted CO_2 was 0.08 ML and 0.03 ML respectively. In this case, reacted CO_2 coverage is equal to the initial oxygen coverage (3.17 ML) minus addition of residual O_2 and CO_2 coverage. The calculation of reacted CO_2 coverage, residual oxygen coverage as well as oxygen coverage consumption percentage for each reaction cycle are listed on the top of each peak in Figure 3-4A. Figure 3-5 shows the IR spectra we collected after each cycle of isothermal oxidation. The bottom one (black) was obtained before the 1^{st} cycle, which corresponds to CO adsorption on pristine PdO(101) surface, whereas the top one (dark blue) was obtained at 100 K under 5×10^{-9} torr CO background after annealing the surface to 900 K, which corresponds to CO adsorption on Pd(111) surface. Based on Figure 3-4A, first three cycles of isothermal CO reaction removed more than half of the oxygen coverage, which leads to the remarkably increase of oxygen vacancy. Furthermore, due to the continuous CO background dosing, we assume that surface was covered by high CO coverage throughout these 7 reaction cycles. As illustrated above, recent DFT calculation suggests that 36% of t-b-t phase and 64% of the all-atop phase compose of CO adsorbing on pristine PdO(101) surface.

Comparing IR of CO adsorbing on pristine PdO(101) surface with IR after 1st cycle reaction, 2132 cm^{-1} atop peak blue shifts and red shifts to 2140 cm^{-1} and 2094 cm^{-1}, respectively. The 2140 cm^{-1} peak is consistent with atop CO adsorbs on oxide phase, broad peak at 2094 cm^{-1} is composed by several peaks overlapped together and is related to atop CO next to oxygen vacancy (N-t) site (Figure 3-3). This assumption is based on the fact that after 1st cycle, 0.463 ML (14.66%) oxygen was reacted, which is more than cus-O (0.35 ML) from the first layer, and due to the diffusion of oxygen atom from deeper layer, we can assume that the surface still remain large domain of PdO(101) with relatively less oxygen vacancy. Note that a small peak appeared at 2111 cm^{-1}, which is consistent with atop CO on Pd(111) (2×2)-3CO compressed phase. This demonstrates a co-existence of metallic and PdO(101) domains during reaction. After 2nd cycle reaction, the intensity of 2140 cm^{-1} peak decreases whereas 2094 cm^{-1} peak blue shifts to 2097 cm^{-1} with almost the same intensity, which indicates the coverage decrease of former type of atop CO and influence of oxygen vacancy on latter type of atop CO. IR spectrum which was collected after 3rd cycle shows that 2140 cm^{-1} peak further blue shifts to 2142 cm^{-1} and diminishes, accompanying with the increase of 2111 cm^{-1} peak. Combining with the information in Figure 3-4A, 52.69% oxygen coverage has been consumed at this time, the change in the spectrum shows that more oxygen vacancies have been generated and Pd(111) regimes increase. From cycle 4 to 7, atop CO peak on oxidized phase has completely disappear and 2111 cm^{-1} is the only dominant peak. Noticed that a small peak at 2095 cm^{-1} appears after fifth cycle, which consists with atop CO on Pd(111) that persists until the (2×2)-3CO phase saturate [39].

As already discussed above, bridging CO in t-b-t phase cause 1953 cm^{-1} peak. After 1st and 2nd reaction cycles, some single oxygen vacancies are formed. In order to reduce the

repulsion, some distribution of atop and bridge CO may cause blue shift of bridging CO from 1953 cm^{-1} to 1969 cm^{-1}. The spectrum collected after 3rd cycle reaction appears a new peak located at 1896 cm^{-1} and Figure 3-4A shows that 52.96% of the oxygen atom has been reacted. Previous DFT calculation [46] mentioned that 1896 cm^{-1} corresponds to the Pd(111) surface hollow site within (2×2)-3CO phase, the appearance of this peak shows that due to the generation of large number of oxygen vacancy, Pd(111) domain has been formed. Besides, a redshift of the peak from 1969 cm^{-1} to 1967 cm^{-1} can be observed. After 4th cycle reaction, oxygen coverage only remained 0.663 ML, which is close to the saturation coverage of 2D oxide. A new peak appears at 2006 cm^{-1}, which matches to the frequency of bridge CO on Pd_5O_4 according to the previous DFT calculation [46]. Furthermore, trailing edge of peak located at 1967 cm^{-1} becomes broad and this trend lasts until to the last reaction cycle.

Summary

In this chapter, we have investigated the RAIRS spectra of CO adsorption on Pd(111), Pd_5O_4, and PdO(101) surfaces as well as isothermal CO oxidation on PdO(101) surface. It turns out that in this case, CO adsorbs on bridge and hollow sites on Pd(111) at the coverage of 0.5 ML at surface temperature 100 K, whereas for Pd_5O_4 and PdO(101) surface, CO mainly adsorbs on a mixture of atop and bridge site that are formed by Pd_{2f} and Pd_{3f}, respectively. In the isothermal CO oxidation experiment, more than 50% of the oxygen coverage is reacted by CO at first 3 cycles, and since then CO adsorption on metal domain within the oxidized surface becomes evident. As the oxygen is almost removed by CO after 7 cycles, IR spectra shows similar peaks comparing with CO adsorption on Pd(111) surface.

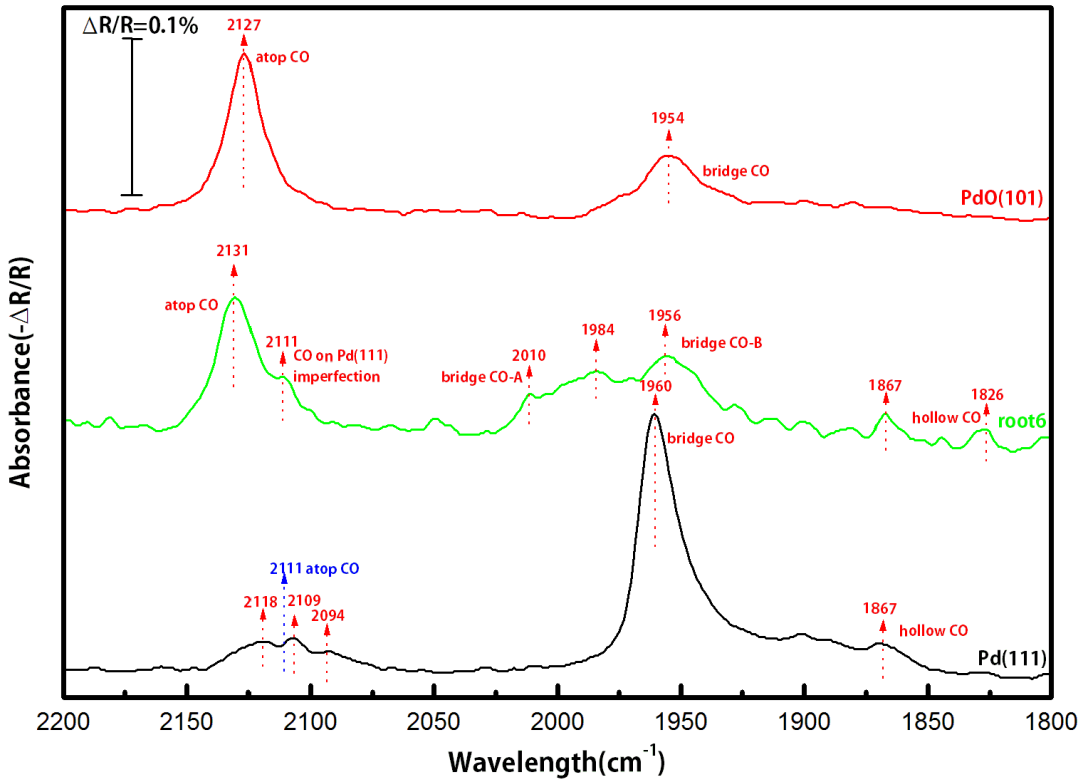

Figure 3-1. RAIRS of CO on Pd(111), Pd_5O_4, PdO(101) surface. IR spectra collected at 100K with 1.0×10^{-8} torr CO background dosing.

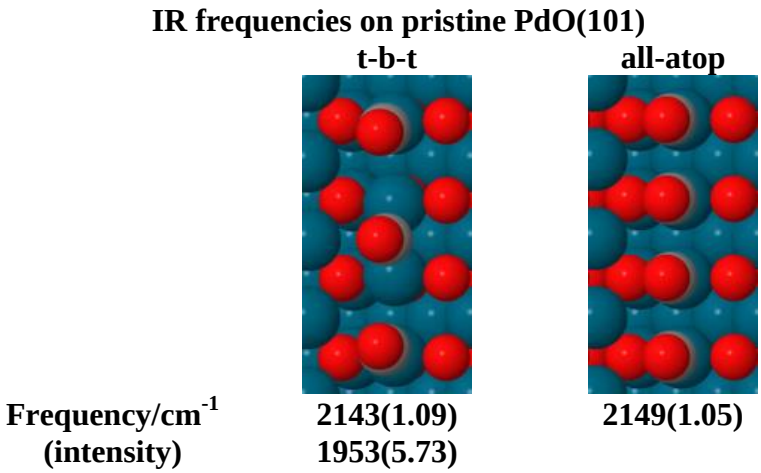

Figure 3-2. IR frequencies (cm^{-1}) and intensities (in parenthesis) of CO on different sites on pristine PdO(101) surface.

IR frequencies on PdO(101) with one oxygen vacancies

	b-t_{Ov}-t	b-t_{Ov}-b	t-t_{Ov}-t	t-t-t_{Ov}	t-t-t_{Ov}-t
	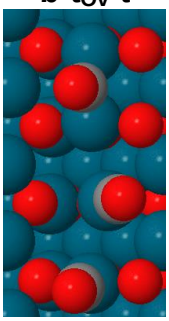	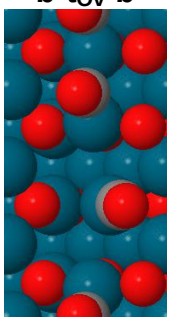	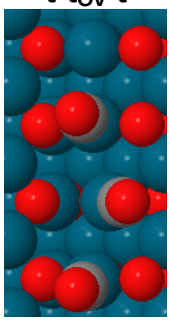	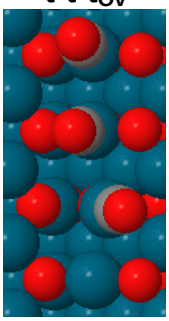	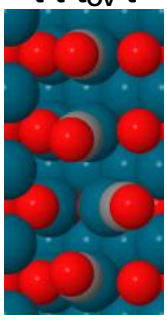
Frequency/cm^{-1} (intensity)	**2139 (0.68)** **2106 (0.26)** **1953 (0.79)**	**2117 (0.55)** **1991 (0.96)** **1967 (0.02)**	**2134 (1.11)** **2119 (0.01)** **2094 (0.12)**	**2135 (1.12)** **2114 (0.02)** **2096 (0.21)**	**2140** **2114** **2078**

Figure 3-3. IR frequencies (cm^{-1}) and intensities (in parenthesis) of CO on different sites on PdO(101) with one oxygen vacancy. For each case, we only take frequencies with large intensities (red) into account.

Figure 3-4. Isothermal CO oxidation on PdO(101) surface and TPD of residual oxygen and CO_2 A) Isothermal CO oxidation on PdO(101) surface at 373K. CO background pressure and dwell time is illustrated in the panel. The CO_2 generation coverage is shown on top of each peak (blue), the remaining oxygen coverage and consumption percentage of total oxygen coverage after each reaction cycle is listed below the CO_2 coverage (green). B) TPD experiment of residual oxygen and CO_2 after stopping the CO background dosing. The coverage of residual O_2 and CO_2 is listed in the panel.

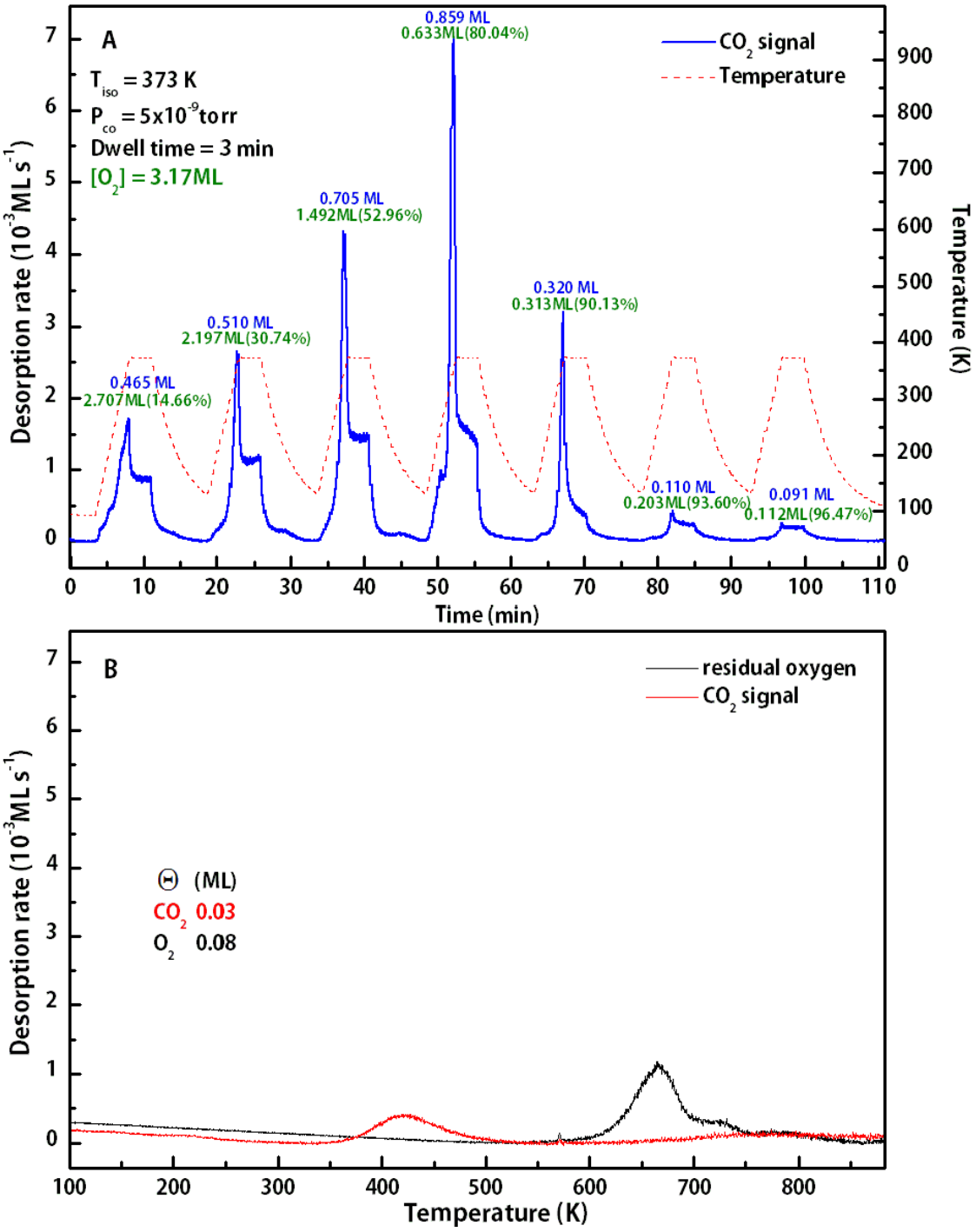
A
T_{iso} = 373 K
P_{co} = 5x10^{-9}torr
Dwell time = 3 min
[O_2] = 3.17ML
CO_2 signal
Temperature
0.465 ML
2.707ML(14.66%)
0.510 ML
2.197ML(30.74%)
0.705 ML
1.492ML(52.96%)
0.859 ML
0.633ML(80.04%)
0.320 ML
0.313ML(90.13%)
0.110 ML
0.203ML(93.60%)
0.091 ML
0.112ML(96.47%)
Desorption rate (10^{-3}ML s^{-1})
Temperature (K)
Time (min)
B
residual oxygen
CO_2 signal
Θ (ML)
CO_2 0.03
O_2 0.08
Desorption rate (10^{-3}ML s^{-1})
Temperature (K)

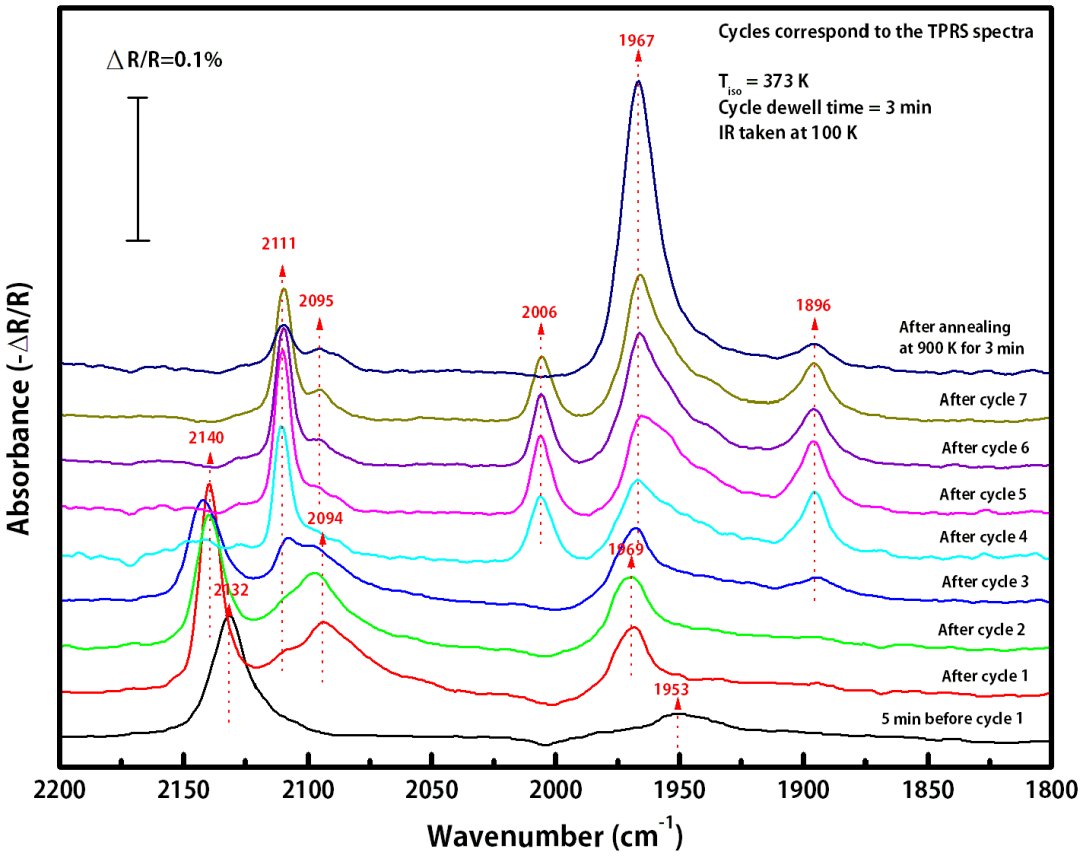

Figure 3-5. Isothermal IR of CO reduction on PdO(101) surface at 373 K. IR was taken at 100 K after each cycle corresponding to the Figure 3-2 (a). The last one (dark blue) was collected at 100 K after annealing the sample to 900 K for 3 minutes and CO background dosing is $P_{co}=5\times10^{-9}$ torr.

CHAPTER 4
CONCLUSION

In conclusion, these studies illustrate utility of atomic oxygen beam in the study of oxidized Pd(111) surface under UHV condition, CO adsorption on metal and oxidized Pd(111) surface as well as CO reduction mechanism on PdO(101) surface. It is evident from current and previous studies that CO adsorption and reaction is both complicated and rich thinking when it comes to the assignment of adsorption sites and geometries of adsorption and reaction structure. Future study will be carried on at: 1) Isothermal reduction of CO on bulk and 2D oxide at high, medium and low temperature. 2) STM studies on real surface for in-situ investigating of CO reaction on metal surface as well as oxidized surface. 3) LEED-AES study of metal and palladium oxide.

LIST OF REFERENCES

[1] D.A. King, Surf. Sci., 47 (1975) 384-402.

[2] P.A. Redhead, Vacuum, 12 203-211.

[3] R.I. Masel, Principles of Adosrption and Reaction on Solid Surfaces, Wiley, New York, 1996.

[4] F. M. Hoffmann, Surf. Sci. 3 (1983) 107

[5] C.J. Zhang, P. Hu, J. Am. Chem. Soc. 123 (2001) 1166.

[6] K. Nakao, S.-I. Ito, K. Tomishige, K. Kunimori, Catal. Today 111 (2006) 316.

[7] H. Gabasch, A. Knop-Gericke, R. Schloegl, M. Borasio, C. Weilach, G. Rupprechter, S. Penner, B. Jenewein, K. Hayek, B. Kloetzer, Phys. Chem. Chem. Phys. 9 (2007) 533.

[8] E.E. Tornau, V. Petrauskas, G. Zvejnieks, Catal. Today 116 (2006) 62.

[9] D. Zemlyanov, B. Aszalos-Kiss, E. Kleimenov, D. Teschner, S. Zafeiratos, M. Haevecker, A. Knop-Gericke, R. Schloegl, H. Gabasch, W. Unterberger, K. Hayek, B. Kloetzer, Surf. Sci. 600 (2006) 983.

[10] H. Gabasch, W. Unterberger, K. Hayek, B. Kloetzer, E. Kleimenov, D. Teschner, S. Zafeiratos, M. Haevecker, A. Knop-Gericke, R. Schloegl, J. Han, F.H. Ribeiro, B. Aszalos-Kiss, T. Curtin, D. Zemlyanov, Surf. Sci. 600 (2006) 2980.

[11] H. Gabasch, W. Unterberger, K. Hayek, B. Kloetzer, G. Kresse, C. Klein, M. Schmid, P. Varga, Surf. Sci. 600 (2005) 205.

[12] B. Klotzer, K. Hayek, C. Konvicka, E. Lundgren, P. Varga, Surf. Sci. 482-485 (2001) 237.

[13] F.P. Leisenberger, G. Koller, M. Sock, S. Surnev, M.G. Ramsey, F.P. Netzer, B. Klotzer, K. Hayek, Surf. Sci. 445 (2000) 380.

[14] E.H. Voogt, A.J.M. Mens, O.L.J. Gijzeman, J.W. Geus, Surf. Sci. 373 (1997) 210.

[15] K.W. Kolasinski, F. Cemic, E. Hasselbrink, Chem. Phys. Lett. 219 (1994) 113.

[16] X. Guo, A. Hoffman, J.T. Yates, Jr., J. Chem. Phys. 90 (1989) 5787.

[17] T. Matsushima, Surf. Sci. 157 (1985) 297.

[18] D. Zemlyanov et al., Surf. Sci. 600 (2006) 983.

[19] H. Gabasch et al., Surf. Sci. 600 (2006) 2980.

[20] B. Klotzer, K. Hayek, C. Konvicka, E. Lundgren, P. Varga, Surf. Sci. 482–485 (2001) 237.

[21] H. Gabasch, W. Unterberger, K. Hayek, B. Kloetzer, G. Kresse, C. Klein, M.Schmid, P. Varga, Surf. Sci. 600 (2005) 205.

[22] X. Guo, A. Hoffman, J.T. Yates Jr., J. Chem. Phys. 90 (1989) 5787.

[23] E.H. Voogt, A.J.M. Mens, O.L.J. Gijzeman, J.W. Geus, Surf. Sci. 373 (1997) 210.

[24] K.W. Kolasinski, F. Cemic, E. Hasselbrink, Chem. Phys. Lett. 219 (1994) 113.

[25] T. Matsushima, Surf. Sci. 157 (1985) 297.

[26] D.L. Weissman-Wenocur, M.L. Shek, P.M. Stefan, I. Lindau, W.E. Spicer, Surf. Sci.127 (1983) 513.

[27] E. Lundgren, G. Kresse, C. Klein, M. Borg, J.N. Andersen, M. De Santis, Y. Gauthier, C. Konvicka, M. Schmid, P. Varga, Phys. Rev. Lett. 88 (2002) 246103/1.

[28] H.H. Kan, J.F. Weaver, Surf. Sci. 602 (2008) L53

[29] H.H. Kan, J.F. Weaver, Surf. Sci. 603 (2009) 2671.

[30] H.H. Kan, J.F. Weaver, Surf. Sci. 602 (2008) 1337.

[31] H. Gabasch, K. Hayek, B. Kloetzer, W. Unterberger, E. Kleimenov, D. Teschner, S. Zafeiratos, M. Haevecker, A. Knop-Gericke, R. Schloegl, B. Aszalos-Kiss, D. Zemlyanov, J. Phys. Chem. C 111 (2007) 7957.

[32] M.S. Chen, Y. Cai, Z. Yan, K.K. Gath, S. Axnanda, D.W. Goodman, Surf. Sci. 601 (2007) 5326.

[33] R.B. Shumbera, H.H. Kan, J.F. Weaver, Surf. Sci. 601 (2007) 4809

[34] G. Zheng, E.I. Altman, Surf. Sci. 462 (2000) 151

[35] S. H. Oh, J. Catal. 124 (1990) 477

[36] N.W. Cant, P.C. Hicks, and B.S. Lennon, J. Catal. 54 (1978) 372

[37] C. H. F. Peden and J.E. Houston, J. Catal. 128 (1991) 405

[38] A.D. Logan and M.T. Paffett, J. Catal. 133 (1992) 179

[39] D.W. Goodman and C. H. F. Peden, J. Phys. Chem. 90 (1986) 4839

[40] J. Gustafson, R. Westerström, O. Balmes, A. Resta, R. van Rijn, X. Torrelles, C.T. Herbschleb, J. W. M. Frenken, E. Lundgren, J. Phys. Chem. C, 114 (2010) 4580

[41] G. Blyholder, J. Phys. Chem. 68 (1964) 2772

[42] D. F. Shriver, P. W. Atkins, C. H. Langford, Inorganic Chemistry, 2nd ed.; Oxford University Press: Oxford/New York, 1994

[43] W. K. Kuhn, J. Szanyi and D.W. Goodman, Surf. Sci. 274 (1992) L611

[44] X. C. Guo and J. T. Yates, J. Chem. Phys. 90 (1989) 6761

[45] A. M. Bradshaw and F. M. Hoffmann, Surf. Sci. 72 (1978) 513

[46] E. Ozensoy, D. C. Meier and D. W. Goodman, J. Phys. Chem. B, 106 (2002) 9367

[47] T. Gie ßel: et al. Surf. Sci. 406 (1998) 90

[48] M. K. Rose, T. Mitsui, J. Dunphy, A. Borg, D. F. Ogletree, M. Salmeron, P. Sautet, Surf. Sci. 512 (2002) 48

[49] N. M. Martin, et al. J. Phys. Chem. C 118 (2014) 1118

[50] J. A., Jr. ,Hinojosa, H.H. Kan, J. F. Weaver, J. Phys. Chem. C 112 (2008) 8324

BIOGRAPHICAL SKETCH

Tao Li earned her BS degree in chemical engineering from Jilin University, China, in 2012, where she did undergraduate research under Dr. Zhan Shi. After graduation, she began her master's studies at the University of Florida in the Department of Chemical Engineering under Dr. Jason F. Weaver in spring 2013. She has coauthored three manuscripts in peer-reviewed journals.